



# Controlled release of dopamine coatings on titanium bidirectionally regulate osteoclastic and osteogenic response behaviors

Mingyue Wang<sup>1</sup>, Chenxi Wang<sup>1</sup>, Yu Zhang<sup>\*</sup>, Ye Lin<sup>\*</sup>

Department of Implantology, Peking University School and Hospital of Stomatology & National Clinical Research Center for Oral Diseases & National Engineering Laboratory for Digital and Material Technology of Stomatology & Beijing Key Laboratory of Digital Stomatology, Beijing 100081, People's Republic of China

## ARTICLE INFO

### Keywords:

Dopamine (DA)  
Titanium  
Implant  
Osteoclast  
Osteogenic  
Alginate-RGD hydrogel

## ABSTRACT

Bone diseases, for example, osteoporosis, cause excessive differentiation of osteoclasts and decreased bone formation, resulting in imbalance of bone remodeling and poor osseointegration, which can be considered a relative contraindication for titanium implants. Dopamine (DA) might provide a solution to this problem by inhibiting osteoclasts and promoting osteoblasts at different concentrations. However, current commercial implants cannot load bone-active molecules, such as DA. Therefore, this study aimed to develop a surface modification method for implants to achieve a controlled release of DA and enhance the resistance of titanium implants to bone resorption and bone regeneration. DA-loaded alginate-arginine-glycine-aspartic acid (RGD) (AlgR) coatings on a vaterite-modified titanium surface were successfully assembled, which continuously and steadily released DA. In vitro studies have shown that materials showing good biocompatibility can not only inhibit receptor activator of nuclear factor-kappa B (NFκB) ligand (RANKL)-induced osteoclastogenesis but also enhance the adhesion and osteogenic differentiation of human bone marrow mesenchymal stem cells (hBMSCs). The optimal DA-loaded concentration of this bidirectional regulation is 100 μM. Interestingly, DA more effectively attenuated osteoclastogenesis when released in a sustained manner from titanium coatings than it did via traditional, free administration, and the alginate-RGD coating and DA clearly exhibited great synergy. This study provides a design of titanium implant surface modification to improve bone remodeling around implants.

## 1. Introduction

Bone remodeling is the dynamic balance between bone resorption and bone formation [1]. Excessive differentiation of osteoclasts affects bone tissue resorption and decreases bone formation, which are common in osteoporosis and other metabolic bone-related diseases [2–4]. This outcome causes poor osseointegration between implants and the surrounding bone tissue, rendering patient recovery difficult [5]. Regulating this imbalance of bone remodeling in bone diseases including inhibiting active osteoclasts around the implants to improve osteogenesis is one of the main methods employed to solve these problems.

Because the systemic administration of drugs with implant placement creates systemic complications and inconvenience for patients, localized strategies such as coating-released molecules usually refrain from systemic drug administration to avoid these limitations [2,6,7]. The localized release of bisphosphonates, one of the most common drug

classes, has been studied as a way to inhibit bone resorption [8–10]. The side effects of oversuppressed bone turnover caused by the systemic administration of bisphosphonates are also likely to occur with improper localized application [11].

Dopamine (DA), the main neurotransmitter in the central nervous system, transmits signals through five G protein-coupled receptors (D1 to D5) to regulate the function of multiple tissues and organs within the brain as well as in other tissues [12,13]. DA has several advantages, such as high loading efficiency in bone repair materials, high biological safety, easy degradation, low-cost synthesis, and suitability for drug delivery, and is a natural, endogenous, small-molecule substance that is related to the nerves of bone marrow [14]. In recent years, great progress has been made in research on DA and its receptors in bone tissue. An increasing number of studies have shown that DA functions in bone tissue in addition to nerves [15–17]. DA receptors are widespread in bone tissues and expressed on the surfaces of osteoclasts, osteoblasts and stem cells [16,18]. By directly affecting receptors on the cell surface, DA

<sup>\*</sup> Corresponding authors at: 22 Zhongguancun South Avenue, Haidian District, Beijing 100081, People's Republic of China.

E-mail addresses: [zhang76yu@163.com](mailto:zhang76yu@163.com) (Y. Zhang), [yorcklin@263.net](mailto:yorcklin@263.net) (Y. Lin).

<sup>1</sup> M.W. and C.W. contributed equally in this work.

can simultaneously enhance osteogenesis by activating DA D1 receptor (D1R) and inhibit osteoclastogenesis by activating DA D2 receptor (D2R), as demonstrated in our earlier research and the research of others [15,16,18]. Considering its moderate osteogenic activity through both osteoblasts and osteoclasts, DA might be used as a small molecule for bone defect repair. In addition, fewer peripheral nerves have been detected around implants compared to natural teeth, and this neurotransmitter has greater potential for implant surface modification. In this study, we load DA onto the surfaces of implants to regulate bone remodeling.

Titanium has fine biocompatibility and mechanical properties, but its surface lacks enough functional groups to promote protein and cell adhesion [19]. Drug-loaded, controlled release systems have been shown to improve cell adhesion, growth and differentiation. Under degenerative conditions, such as those in osteoporosis, surface-modified and drug-loaded implants undoubtedly show better osseointegration than implants alone [5]. Recently, due to their biocompatibility, wettability and adjustability, polymer hydrogels have received extensive attention for their use as coatings on titanium materials [20–22]. Hydrogels have been successfully utilized in tissue engineering because their microstructure is similar to the natural extracellular microenvironment and due to their characteristic porosity and ability to be easily formed and processed, which is conducive to cell growth and tissue regeneration [23–25]. Interstitial pores can be used to load therapeutic drugs and help drug molecules diffuse in the tissue or surrounding cells [26]. In addition, hydrogels used as coatings provide a three-dimensional (3D) soft material-based interface, which can increase the ability to immobilize proteins compared to that with flat 2D coatings [27]. Hence, titanium coated with hydrogels combines the excellent properties of titanium (biocompatibility and mechanical properties) with the excellent properties of hydrogels (hydrophilicity, lubricity, biocompatibility, and drug storage and release behaviors) [21].

The purpose of this research was to create a hydrogel-coated titanium implant to carry out sustained, controlled release of DA into the microenvironment and to explore its regulatory effect on bone remodeling and the optimal concentration of DA. This bioactive coating could improve the ability of the titanium surface to resist bone resorption and penetrate the bone tissue and thus shows good prospects for inhibiting osteoclast formation and resorption and promoting bone regeneration.

## 2. Materials and methods

### 2.1. Materials

DA hydrochloride, sodium alginate, calcium chloride ( $\text{CaCl}_2$ ,  $\geq 99.0\%$ ) and sodium carbonate ( $\text{NaCO}_3$ ,  $\geq 99.5\%$ ) powders, SKF-38393 ( $\geq 98\%$ ) and pramipexole ( $> 98\%$ ) were purchased from Sigma-Aldrich (St. Louis, MO, USA). 2-(*N*-morpholino)ethanesulfonic acid (MES,  $\geq 99.5\%$ ), *N*-(3-dimethylaminopropyl)-*N'*-ethylcarbodiimide (EDC, 98.0%), *N*-hydroxysulfosuccinimide (sulfo-NHS, 98%) and hydroxylamine ( $\text{NH}_2\text{OH}$ ) solutions (50 wt% in  $\text{H}_2\text{O}$ ) were obtained from Aladdin Reagent Co. Ltd. (Shanghai, China). The arginine-glycine-aspartic acid (RGD) peptide with a sequence of (glycine)<sub>4</sub>-arginine-glycine-aspartic acid-serine-proline (abbreviated G<sub>4</sub>RGDSP, 97.1% purity) was purchased from Chinese Peptide Co., Ltd. (Hangzhou, China).

### 2.2. Fabrication of an alginate-RGD@DA hydrogel precursor solution

Sodium alginate (ratio of guluronic acid to mannuronic acid (M/G) = 1.56) was selected for alginate-RGD (AlgR) synthesis. Using published carbodiimide chemistry methods, covalent coupling of the RGD peptide with an alginate polymer was performed, as described by Rowley et al. [28] Briefly, sodium alginate was dissolved in 0.1 M MES buffer (pH 6.5, 0.3 M NaCl) at a final concentration of 1% w/v and stirred overnight at room temperature. To each gram of alginate, 27.4 mg of sulfo-NHS, 48.42 mg of EDC, and 16.7 mg of RGD peptide were added. The

reaction was stirred at room temperature for 20 h and then quenched with an appropriate amount of  $\text{NH}_2\text{OH}$ . The alginate mixture was then transferred to a prewetted 3.5-kDa MWCO (Spectra/Por S) dialysis membrane, dialyzed against buffer with a reduced salt concentration over 5 days, sterile filtered with a 0.22- $\mu\text{m}$  filter, frozen, lyophilized, and stored at  $-80^\circ\text{C}$  until use. A DA solution with sodium alginate or lyophilized sodium AlgR was added to form 2% Alg and AlgR, which were dissolved overnight in a  $37^\circ\text{C}$  incubator to obtain hydrogel precursor solutions.

### 2.3. Preparation of hydrogel-coated titanium

Commercial pure titanium sheets (grade 2, purity  $> 99.6\%$ , diameter of 15 mm and thickness of 1 mm, Baoji, China) were used in this work. First, the titanium sheets were polished with silicon carbide sandpaper (#240–#2000) and then ultrasonically cleaned with acetone, absolute ethanol, and deionized water, after which the material was defined as Ti. Thereafter, the Ti sheets were sandblasted with  $\text{Al}_2\text{O}_3$  particles (diameter of 0.25–0.5 mm), followed by etching using  $\text{HCl}/\text{H}_2\text{SO}_4$  to increase the roughness, after which the material was defined as SLA titanium.

Calcium carbonate ( $\text{CaCO}_3$ ) was then formed on the surface of the SLA titanium using the  $\text{CaCO}_3$  crystallization method developed by Savelyeva et al. [29] Briefly, the  $\text{CaCO}_3$  coating was formed by chemical precipitation of 0.33 M  $\text{CaCl}_2$  and 0.33 M  $\text{NaCO}_3$  solutions. Before the mineralization process, the SLA titanium sheets were sonicated in a  $\text{CaCl}_2$  solution for 10 min, after which an equal volume (1 mL) of a  $\text{NaCO}_3$  solution was added, and ultrasonication (US) was performed for 30 s ( $20^\circ\text{C}$  and 40 Hz). The mixture was allowed to rest in a Petri dish for 1 min to complete the crystallization process, followed by 3 wash steps with deionized water. The abovementioned precipitation step was repeated once. The samples were sterilized in an autoclave ( $120^\circ\text{C}$  and 30 min) to obtain SLA/ $\text{CaCO}_3$  titanium.

To form a hydrogel coating on the surface of SLA/ $\text{CaCO}_3$ , 70  $\mu\text{L}$  of hydrogel precursor solution (Alg, AlgR or AlgR@DA) was loaded on the interface and incubated for 10 min. Thereafter, the treated samples were immersed in 2 mL of a  $\text{CaCl}_2$  solution (0.5 M) for 10 min to crosslink the hydrogel. The treated samples were washed 3 times with phosphate buffer saline (PBS) to remove excess  $\text{Ca}^{2+}$  ions.

### 2.4. Physicochemical property analyses

Scanning electron microscopy (SEM) (S-3000N, Hitachi, Germany) and a 3D optical microscope were employed to observe the different interfaces. The average interface roughness (Ra) and surface roughness (Sa) values were calculated. The contact angle test was conducted to check the hydrophilicity by dropping 10  $\mu\text{L}$  of deionized water onto the surface. This measurement was carried out with a contact angle system (OCA-20, DataPhysics, Germany). The average water contact angle (WCA) was evaluated for the 3 samples in each group. Fourier transform infrared (FTIR) spectroscopy was performed using an FTIR spectrometer (Nicolet IS10, USA). After each group of coatings had naturally dried, the chemical compositions and changes in the chemical bonds in the coatings were detected. Each spectrum was collected from 400 to 4000  $\text{cm}^{-1}$  at a resolution of 0.4  $\text{cm}^{-1}$  through 25 scans. The crystalline phases of the coatings were identified using an X-ray diffraction (XRD) instrument (Bruker D8 Advance, Japan). The diffractograms were scanned in  $2\theta$  ranges from  $20^\circ$  to  $60^\circ$  at a step rate of  $0.02^\circ/\text{s}$ . The hydrogel-titanium binding strength was tested by the lap-shear adhesion test, in which the surfaces of two  $\text{CaCO}_3$ -modified SLA titanium plates were bonded using a 2-mm-thick hydrogel layer and pulled apart with a Tensirech testing system equipped with a 3-kN load cell. There were 3 replicates for each group.

## 2.5. DA release profile testing by high-performance liquid chromatography (HPLC)

High-performance liquid chromatography (HPLC) was used to measure the release of DA from AlgR@DA coatings using an Xselect T3 column (250 × 4.6 mm, 5 μm, Waters, USA). The mobile phase was 0.1% phosphoric acid/acetonitrile (9:1), and the number of theoretical plates exceeded 3000. The flow rate was 0.8 mL/min, and the detection wavelength was 280 nm. The column temperature was 35 °C, and the injection volume was 15 μL. The dialysis bag method was applied to assess the release of DA from the AlgR@DA coating in vitro. The release of DA from modified titanium sheets was analyzed at 37 °C in PBS at various pH values (pH 6.5, 7.4 and 8.0). One milliliter of the release media was obtained at each indicated time point and used to measure the DA content and simultaneously supplement the release media. External media were replaced every other day, at which time the cumulative release amount was calculated, and the release curve was drawn.

## 2.6. Culture and differentiation of RAW264.7 osteoclast precursor cells

RAW264.7 cells, which comprise a murine, osteoclast, precursor macrophage cell line, were purchased from Peking Union Medical College (Beijing, China). The cells were cultured in Dulbecco's modified Eagle's medium (DMEM) supplemented with 10% fetal bovine serum (FBS) and placed in a humidified incubator with 5% CO<sub>2</sub> at 37 °C. The osteoclast differentiation media consisted of DMEM containing 10 ng/mL receptor activator of nuclear factor-kappa B (NFκB) ligand (RANKL) (R&D Systems) and 10% FBS. Cell fusion was observed under a light microscope. RAW264.7 cells on the interfaces in which osteoclast differentiation had been successfully induced and osteoclasts were identified by cells with 3 or more nuclei and by typical osteoclasts.

## 2.7. Proliferation assays of RAW264.7 cells

RAW264.7 cells were seeded on the materials at a density of  $3 \times 10^4$  cells/well, with 5 replicates in each group for 1, 4, and 7 days. The media in each well were replaced with 10% CCK-8 reagent (Dojindo, Japan), and the cells were incubated for 2 h at 37 °C in the dark. Afterwards, the supernatant was aspirated and added to a 96-well plate, and the optical density (OD) of each well at 450 nm was measured using an ELx808 multifunction microplate reader (BioTex, Winooski, VT), with the values from multiple wells averaged in each group. Furthermore, a fluorescent live/dead viability assay kit (KeyGEN BiOTECH, China) was employed to evaluate cell viability. Briefly, a fluorescent dye solution containing 8 μM propidium iodide (PI) and 2 μM calcein-AM in PBS was utilized to replace the media in each well, after which cells were incubated at 37 °C in the dark for 15 min. Live cells were stained green with calcein-AM (490 nm), while PI-stained dead cells were stained red (535 nm). To determine cell viability, the ratio of live/dead cells was calculated in 10 random fields per sample ( $n = 3$ ).

## 2.8. TRAP staining and TRAP activity assay

Tartrate-resistant acid phosphatase (TRAP) staining was conducted with an acid phosphatase leukocyte staining kit (Sigma) according to the manufacturer's protocol. TRAP-positive cells with 3 or more nuclei were regarded as osteoclasts. To determine TRAP activity, the cells were washed twice with PBS and lysed by radioimmunoprecipitation assay (RIPA) lysis buffer at 4 °C. The supernatant was collected, and the TRAP Assay Kit (Beyotime, China) was selected to measure the TRAP activity according to the manufacturer's instructions.

## 2.9. Cytoskeleton staining

To further observe the effect of DA administration through

controlled release from the hydrogel coating on the formation of osteoclasts, immunofluorescence staining of the F-actin ring was performed, as previously reported [30]. After 2 days of culture with RANKL, cells grown on interfaces were fixed with 4% paraformaldehyde for 15 min and washed twice with PBS at room temperature. Afterwards, the cells were stained with 0.1% phalloidin (Abcam) and ProLong® Gold Antifade Reagent with 4',6-diamidino-2-phenylindole (DAPI) (cell signaling technology (CST)) according to the manufacturers' protocols. Immunofluorescence images were captured with a laser scanning confocal microscope (LMS710, Zeiss, Germany).

## 2.10. Immunofluorescence staining

RAW264.7 cells were plated on interfaces at a density of  $3 \times 10^4$  cells/well, cultured with RANKL for 4 days, and then fixed with paraformaldehyde (4%) for 30 min. Afterward, the cells were permeabilized with Triton X-100 (0.1%) for 5 min and blocked with 5% goat serum for 30 min at room temperature. Alexa Fluor488-conjugated anti-NFATc1 antibody (1:200, Biolegend) was incubated for 1 h at 4 °C. The nuclei were stained with DAPI. Images were obtained with a confocal microscope.

## 2.11. Total RNA isolation and quantitative real-time PCR (qRT-PCR)

To evaluate gene transcription in cells at the interfaces, total RNA was isolated using TRIzol reagent (Invitrogen, USA). An ultraviolet (UV) spectrophotometer was used to detect the RNA concentration and purity, and only samples with an absorbance ratio (260/280 ratio) >1.8 were selected for subsequent experiments. mRNA was reverse transcribed into cDNA using aPrimeScript RT Kit (Takara, Japan) according to the manufacturer's instructions. Quantitative real-time polymerase chain reaction (qRT-PCR) was carried out with an ABI 7500 RT-PCR system (Applied Biosystems, USA). Glyceraldehyde-3-phosphate dehydrogenase (GAPDH) mRNA served as an internal control. Table S1 lists the primer sequences in this study. The  $2^{-\Delta\Delta Ct}$  method was employed to determine relative gene expression levels.

## 2.12. Protein extraction and western blot analysis

After 7 days of culture with RANKL, cells were lysed in RIPA buffer (Sigma Aldrich, USA) with a protease inhibitor cocktail (Solarbio, China) for 30 min. A bicinchoninic acid (BCA) protein assay kit (Thermo, USA) was used to quantify the total protein content of the lysates. Proteins were separated by sodium dodecyl sulfate-polyacrylamide gel electrophoresis (SDS-PAGE) and transferred to polyvinylidene fluoride (PVDF) membranes (Millipore, USA). After blocking with skim milk (5%) in (tris-buffered saline with 0.1% Tween 20) TBST for 1 h, membranes were incubated with rabbit primary antibodies including NFATc1, β-actin, p-AKT, t-AKT, p-NFκB, t-NFκB, p-PKA, t-PKA, p-CREB, and t-CREB (Abclonal, China) overnight at 4 °C. The blots were then visualized with an ECL detection kit (CWBI, China) after incubation with horseradish peroxidase (HRP)-conjugated secondary antibodies. ImageJ software was employed to measure the gray value for each target protein band.

## 2.13. Culture of hBMSCs

Human bone marrow mesenchymal stem cells (hBMSCs) were obtained from ScienCell Company (San Diego, CA). The cells were cultured in α-Minimal Essential Medium (MEM) supplemented with 10% FBS, 100 U/mL penicillin G and 100 mg/mL streptomycin (Gibco, Grand Island, NY). The media were replaced every 2–3 days. Cells at passages 5–6 were employed for the experiments.

## 2.14. Proliferation and morphologies of hBMSCs

The morphology of the hBMSCs cultured on the hydrogel-coated titanium sheet was examined by SEM (SU-8020, Hitachi, Japan) of the sample dried at the critical point. The proliferation and morphology of the hBMSCs were examined by CCK-8 and live/dead staining.

## 2.15. Osteogenic differentiation of hBMSCs

For osteoinduction, hBMSCs were seeded onto different interfaces at a density of  $2 \times 10^4$ /well. After the hBMSCs were 70–80% confluent, the media were replaced with osteogenic media (OriCell™ hMSC Osteogenic Differentiation Media, Cyagen Biosciences, China) and changed every 3–4 days. After 7 and 14 days of osteoinduction, osteogenic differentiation was evaluated by alkaline phosphatase (ALP) activity using an ALP activity kit (JianCheng Bioengineering Institute, China). The results were normalized to the levels of total protein, which were measured by a BCA Kit.

## 2.16. Statistical analyses

All data were analyzed in triplicate and are expressed as the mean  $\pm$  standard deviation. Student's *t*-test or one-way analysis of variance (ANOVA) followed by Tukey's post hoc test was performed using SPSS 25.0 software.

## 3. Results and discussion

### 3.1. Preparation of DA-loaded bioactive hydrogel coatings on titanium

A schematic of the entire surface engineering process utilized for stepwise assembly of the biological interface on the Ti surface is shown in Fig. 1.

- (1) The titanium surface was roughened by sandblasting and acid etching, the most commonly applied clinical titanium roughening treatments [31]. High surface roughness is crucial for the adhesion of a hydrogel layer to a titanium substrate [32].
- (2) The SLA Ti samples were further modified by in situ  $\text{CaCO}_3$  mineralization. In recent years, many studies to improve the adhesion of hydrogel coating materials to metal substrates have been conducted [32,33]. Due to the inertness of coatings and the poor adhesion of coatings to the Ti surface, complex physical and chemical methods, such as pulsed laser deposition (PLD), plasma spray deposition (PSD), electrophoretic deposition (ED), and strong chemical etching are usually required to deposit coatings

[20,34,35]. Recent studies have assessed the introduction of covalent bonds between hydrogels and titanium [33,36]. However, this strategy requires complex physical or chemical surface modification and is suitable for hydrogels containing only specific functional groups, such as methacrylate and acrylate. The latest research indicated that a  $\text{CaCO}_3$  layer fabricated at the hydrogel-titanium interface can act as a “binder” to increase the surface roughness through positively charged  $\text{Ca}^{2+}$  ions and negatively charged  $\text{TiO}$ , tightly attaching the hydrogel to the titanium surface through bonds between the sites [37,38]. Additionally, mineral crystals can grow inside alginate hydrogels and then bind the polymer network to achieve a firm interface bond [38]. The  $\text{CaCO}_3$  layer significantly enhances interfacial bonding between hydrogels and titanium. This strategy does not require complex chemical or physical surface modification; therefore, it shows good performance in a wide range of biomedical applications in the field of hydrogel-titanium hybrids. Here, in situ mineralization of  $\text{CaCO}_3$  was selected to enhance the adhesion of titanium to the hydrogel coating.

- (3) Sodium alginate was grafted with an adhesion peptide with an RGD sequence with carbodiimide. Alginate is widely utilized in many biomedical applications, such as tissue regeneration, drug delivery, and cell encapsulation properties, due to its high biocompatibility, low toxicity, and relatively low cost [39]. Alginate is rich in calcium-binding groups (such as carboxyl groups), which can serve as nucleation sites for the growth of Ca–P crystals [40]. In addition, a study showed that alginate itself has bone-stimulating properties and increased bone density on titanium implants and tissue scaffolds compared to that of the corresponding control [41]. Because of the diverse advantages and drug-loading properties of alginate, we expect its use for the biologically active coating of titanium implants to achieve the controlled release of DA. Cells do not have receptors for alginate polymers, and extracellular matrix (ECM) proteins are not easily absorbed onto the hydrophilic surface of hydrogels [28]. Integrins are the main family of cell/surface adhesion receptors that bind adhesion ligands (for example, a peptide containing Arg-Gly-Asp [RGD]) [42]. The binding of integrins to individual ligands is relatively weak. However, when integrins aggregate and bind ligands in the same area, considerable cell adhesion is generated, forming focal adhesions. These focal adhesions recruit and control signaling molecules involved in differentiation, proliferation, and proliferation [43,44]. Therefore, RGD peptides are usually coupled to alginate polymer chains to enhance cell adhesion and viability [23]. Here, we proposed grafting RGD onto a sodium alginate hydrogel to support cell adhesion and

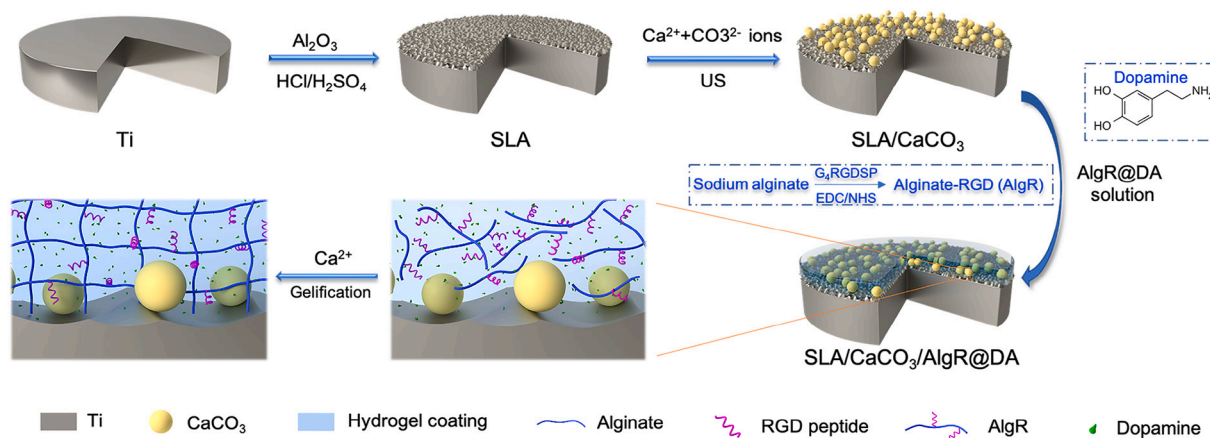


Fig. 1. Schematic of the step-by-step fabrication of AlgR@DA hydrogel coatings by the  $\text{CaCO}_3$  mineralization of SLA titanium surfaces. (US: ultrasonication, 20 °C, 40 Hz).

diffusion. By covalently coupling the RGD peptide to an alginate polymer chain, it was possible to create cell adhesion sites, enhance the binding of cells and alginate, promote cell attachment, and cause cells to adhere to the surface of the material and receive DA stimulation, thereby changing the regulation of cell processes.

(4) Subsequently, DA was added to the RGD-treated alginate solution by thorough mixing. The DA-loaded, RGD-grafted, sodium

alginate solution was evenly coated on the surface of the CaCO<sub>3</sub>-modified SLA to achieve hydrogel precursor coating.

(5) The hydrogel was crosslinked in solution. In this study, hydrogels were prepared by immersing hydrogel-coated titanium sheets with CaCl<sub>2</sub>. The guluronate block of one alginate chain was combined with that of the other alginate chain for crosslinking, generating a gel structure [45].

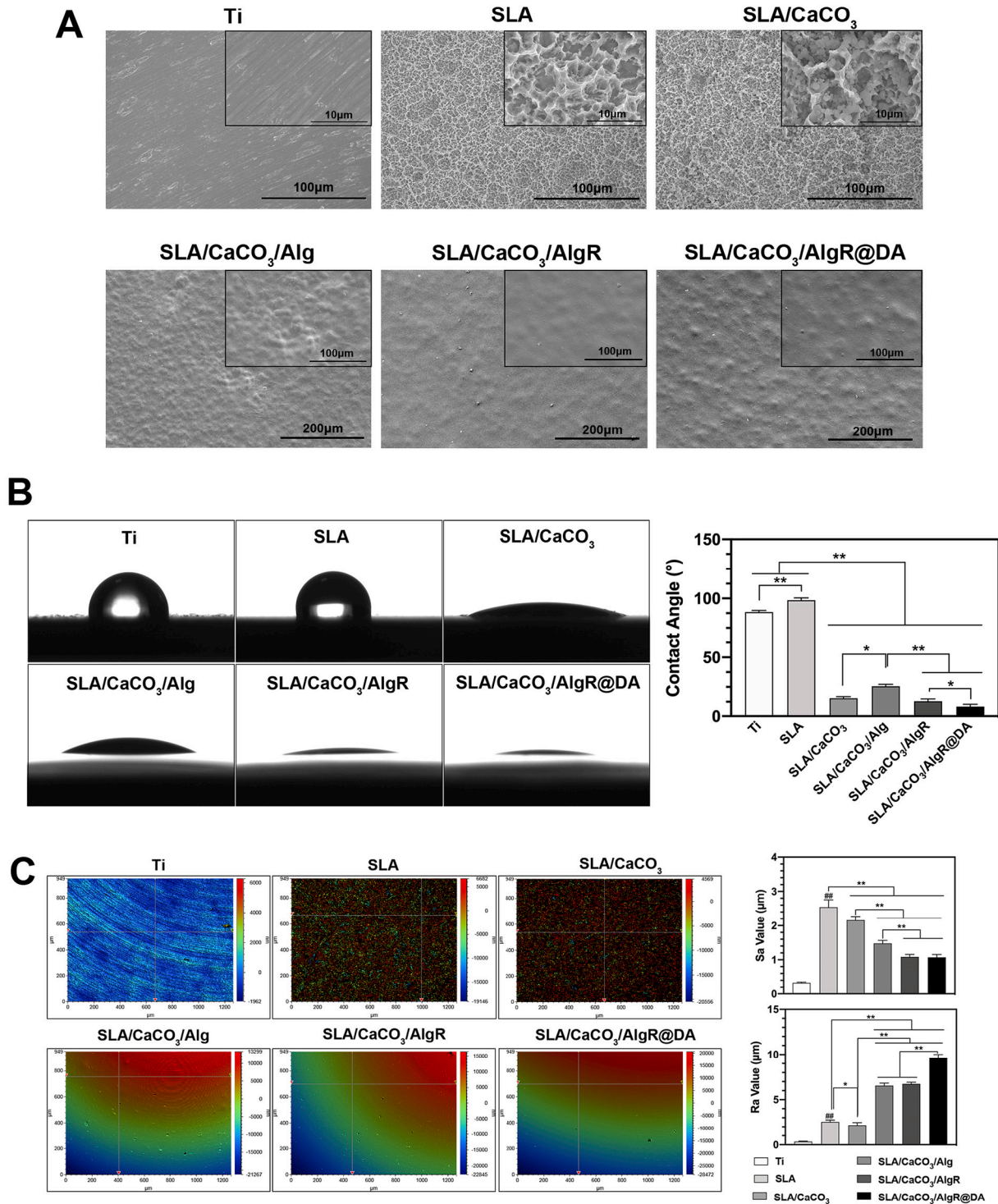


**Fig. 2.** SEM (A), WCA (B) and 2D optical microscopy images (C) of Ti, SLA, SLA/CaCO<sub>3</sub>, SLA/CaCO<sub>3</sub>/Alg, SLA/CaCO<sub>3</sub>/AlgR, SLA/CaCO<sub>3</sub>/AlgR@DA and the quantitative results for each group (\**p* < 0.05, \*\**p* < 0.01; ##*p* < 0.01, relative to Ti group).

### 3.2. Physical and chemical properties of engineered titanium

The morphology of the modified titanium was characterized by SEM (Fig. 2A). The SLA surface obtained by sandblasting and acid etching showed a porous surface with pits with a depth range of several micrometers to tens of micrometers. Schwartz et al. showed that a rough surface provides an interlocking structure with hard tissues and improves osteointegration between the bone and the implant material [46]. Porous spherical vaterite  $\text{CaCO}_3$  particles were formed in the form of particle aggregates in micron-scale pits.  $\text{CaCO}_3$  easily nucleated on the titanium surface. Calcium ions accumulated on the titanium surface due to electrostatic bonding. The vaterite layer, which can be regarded as an adhesive that bonds the hydrogel to the solid substrate and anchors the hydrogel to the titanium surface, can significantly enhance interfacial bonding between the hydrogel and the titanium substrate [38]. The EDX analysis results of the elemental chemical composition of the SLA/ $\text{CaCO}_3$ /AlgR@DA matrix are shown in Fig. S1. The existence of Ca, C, O and Cl was confirmed, and trace amounts of N were detected, indicating that  $\text{CaCO}_3$ , calcium alginate and DA were deposited on the titanium surface.

After fabrication of the hydrogel coating, the interfaces showed uniform spherical protrusions, with uniformly dispersed, spherical, vaterite crystals underneath, with SEM. The porous structure of the hydrogel coatings was difficult to observe due to collapse.

In addition, the WCAs of the interfaces are widely applied to provide information about the wettability and surface energy of biological materials [47]. The results in Fig. 2B show that the WCA of the SLA surface decreased from  $98.51 \pm 1.93^\circ$  to  $15.58 \pm 1.28^\circ$  upon modification with  $\text{CaCO}_3$ . Modification with the RGD peptide ( $13.07 \pm 1.89^\circ$ ) and DA ( $8.59 \pm 1.98^\circ$ ) increased the hydrophilicity of the material, while the hydrophilicity of the SLA surface coated with alginate without RGD modification ( $25.56 \pm 1.73^\circ$ ) was inferior to that of the  $\text{CaCO}_3$ -modified SLA surface. This change in hydrophilicity was due to the superhydrophilic properties of the RGD peptide and DA, which might affect cell adhesion and recognition.

Surface roughness data and 2D images of the samples were obtained through an optical microscope (Contour GT, Bruker). Vision64 software was applied to analyze the roughness data. By calculating the Ra and Sa, hydrogel coating-modified titanium was determined to have a higher Ra value, and the DA-loaded group had the highest Ra value ( $9.66 \mu\text{m}$ ) and a Sa value of  $1\text{--}2 \mu\text{m}$  (Fig. 2C). The presence of a certain degree of roughness (Sa should fall in the range  $1\text{--}2 \mu\text{m}$ ) and micron-scale morphology could activate the interaction of integrin receptors on the surface of specific osteoblast membranes with bone matrix proteins,

thereby affecting the biological activity of the cells [48].

In the FTIR spectrum, the characteristic peaks for Ti and SLA (Fig. 3A) at  $482 \text{ cm}^{-1}$  and  $436 \text{ cm}^{-1}$  were designated as the stretching vibration peaks of Ti—O. The characteristic alginate peaks were clearly observed for the mixed material scraped from the substrate of the  $\text{CaCO}_3$ -modified SLA [49]. The stretching vibration peak characteristic of the OH functional group was observed at  $3343 \text{ cm}^{-1}$ , and the CH  $\text{cm}^{-1}$  stretching band appeared at a wavenumber of  $2928 \text{ cm}^{-1}$ . The C=O stretching vibration peak at  $1597 \text{ cm}^{-1}$  was observed; a peak at  $1426 \text{ cm}^{-1}$ , the symmetrical peak for the COOH stretching vibration peaks, was also observed. Additionally, stretching vibration peaks from the CO bond were observed at  $1078 \text{ cm}^{-1}$  and  $1010 \text{ cm}^{-1}$ . In addition, the observed peak at  $876 \text{ cm}^{-1}$  confirmed the adherence of  $\text{CaCO}_3$  to the internal surface of the hydrogel coatings [37]. For RGD-modified calcium alginate, a peak ( $1510 \text{ cm}^{-1}$ ) characteristic of the amine group (amide II band) was observed, indicating that the RGD peptide, which contains a large number of amine groups, was introduced by grafting [50]. The characteristic DA peak overlapped with the alginate peak, so the spectrum of the AlgR@DA group was similar to that of the AlgR group [51].

The results of XRD analysis to determine the crystallinity of the coatings are shown in Fig. 3B. Ti displayed signals with  $2\theta$  values of approximately  $35^\circ$ ,  $38^\circ$ ,  $40^\circ$ , and  $53^\circ$ . After sandblasting and acid etching, the chemical composition of the porous surface layer also changed to rutile  $\text{TiO}_2$  ( $2\theta$  values of approximately  $27^\circ$ ,  $36^\circ$ ,  $54^\circ$ ). After in situ mineralization and  $\text{CaCO}_3$  modification, peaks indicating vaterite polycrystals appeared at  $2\theta$  values  $\approx 25^\circ$ ,  $27^\circ$ ,  $33^\circ$ ,  $44^\circ$  and  $51^\circ$ , and a small peak indicating rhombus calcite appeared at  $\approx 29^\circ$  [37]. This finding was consistent with our FTIR spectroscopy results. The XRD pattern with the hydrogel coatings was similar to that of the  $\text{CaCO}_3$ -modified SLA, which showed only the vaterite crystal peak, indicating that the composition in the coating was amorphous.

### 3.3. Bonding strength of the hydrogel coatings

Taking into account the working conditions of the implant, we found that achieving improved adhesion to the Ti surface in a humid environment is critical to the successful use of multifunctional hydrogel coatings on Ti implants. The adhesive strength of the  $\text{CaCO}_3$ -modified SLA titanium surface grafted with the hydrogel was evaluated by the lap-shear adhesion test. In the test, a  $200\text{-}\mu\text{L}$  alginate hydrogel layer was applied to bond two titanium plates (area of  $25 \text{ mm} \times 25 \text{ mm}$ ), and a tensile tester was utilized to pull them apart. The load/position curve is shown in Fig. 4A. The peak force load was defined as the highest point of

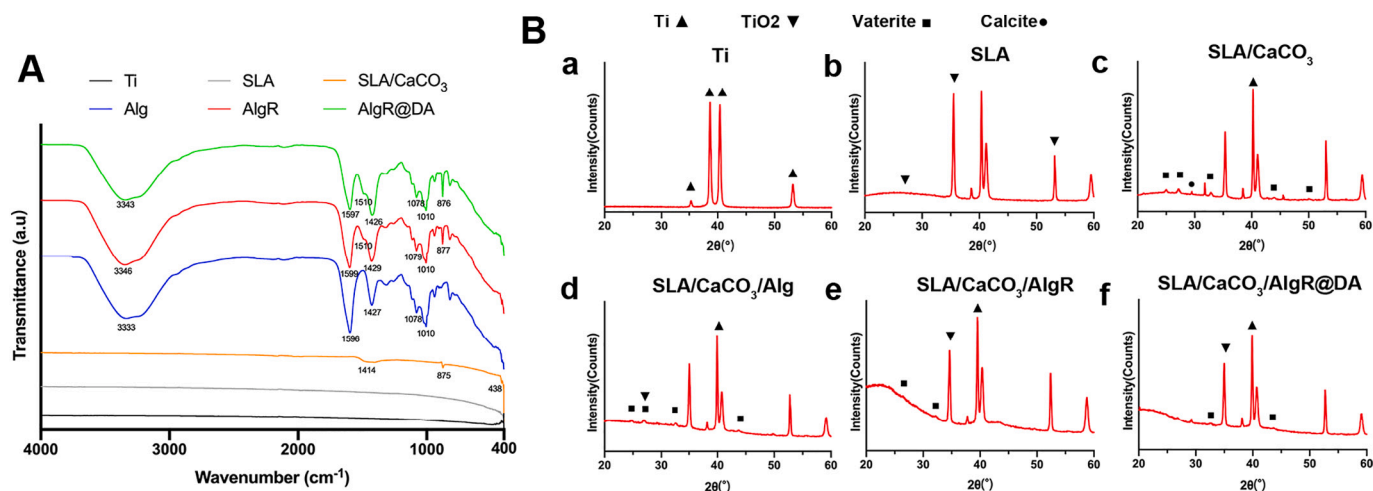
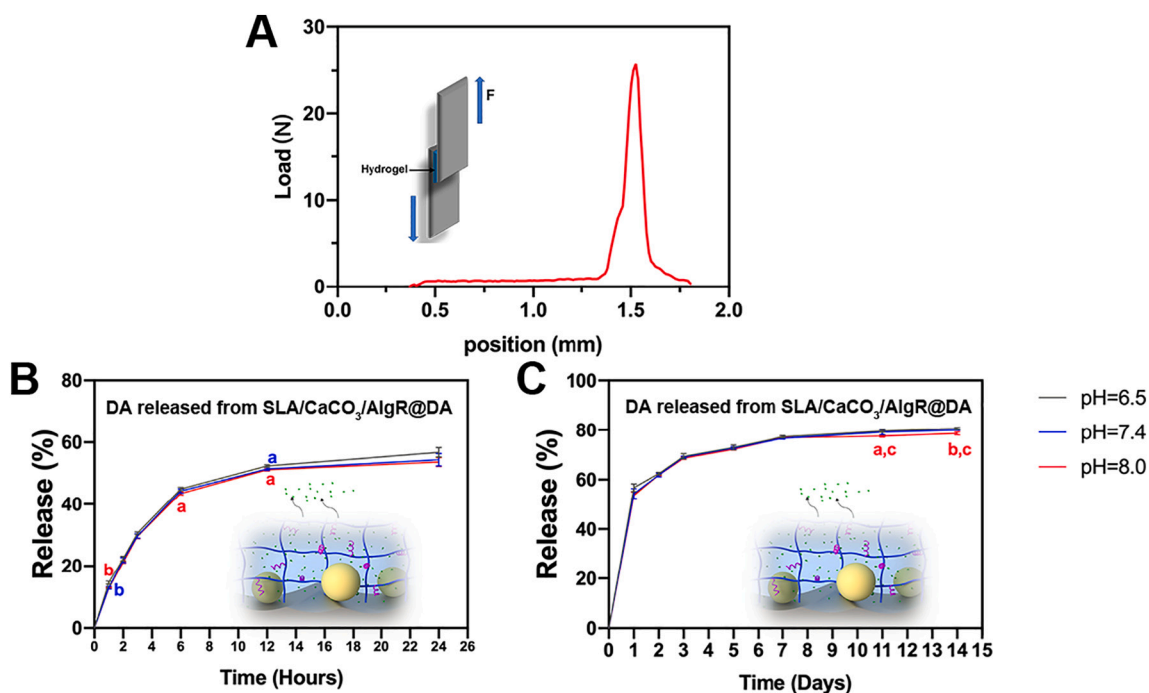


Fig. 3. FTIR spectra (A) and X-ray diffraction (XRD) patterns (B) of Ti (a), SLA (b), SLA/ $\text{CaCO}_3$  (c), SLA/ $\text{CaCO}_3$ /Alg (d), SLA/ $\text{CaCO}_3$ /AlgR (e) and SLA/ $\text{CaCO}_3$ /AlgR@DA (f).



**Fig. 4.** Adhesive strength and release profiles of hydrogel coatings. (A) Load versus position data obtained from the lap-shear test involving the formation of Ca-Alg between SLA/CaCO<sub>3</sub> titanium sheets. (B–C) DA release profile from SLA/CaCO<sub>3</sub>/AlgR@DA determined by HPLC (a:  $p < 0.05$  vs pH = 6.5; b:  $p < 0.01$  vs pH = 6.5; c:  $p < 0.05$  vs pH = 7.4).

the perceived peak of the force-displacement curve and represented bond failure between the hydrogel and the titanium. Shear strength was calculated by using the peak force ratio of the contact area of the hydrogel and titanium plate and applied to evaluate the bonding strength of the hydrogel and titanium. The results showed a shear strength of 41.5 kPa after 10 min of Ca<sup>2+</sup> crosslinking. The vaterite crystals formed a continuous mineral layer at the interface, thereby expanding the contact area of the titanium substrate and enhancing the bonding strength. The maximum bond strength (approximately 41.5 kPa) mainly depends on the mechanical strength of the hydrogel because during the lap-shear test, due to cohesive failure of the massive hydrogel, the hydrogel-titanium interface bond is broken [38]. Hydrogels with lower strength exhibited lower shear adhesion and were considered to provide the required shear adhesion by increasing the concentration of the hydrogel or crosslinking agent [52].

### 3.4. Release profiles of DA from hydrogel coatings

In the process of bone defect repair, different cells have different effects on the pH of the microenvironment. Osteoclasts are present in an acidic environment (pH = 5.0–6.5), and the microenvironment of osteoblasts is slightly alkaline (pH = 7.4–8.5) [53]. Therefore, the release profiles of DA from the coatings at various pH values (6.5, 7.4 and 8.0) were analyzed. With the previously described method, HPLC was employed to detect the release of DA from DA-loaded hydrogel coatings [54]. The results in Fig. 4B show that DA underwent burst release in the early stage, during which approximately 50% of the DA was released within 24 h. The release in the first 12 h was slightly faster than that at pH = 7.4 and weakly alkaline in a weakly acidic environment. No significant difference was observed in the release profiles of DA between pH = 7.4 and pH = 8.0. This early burst release may be conducive to cell adhesion [55]. Later, the relatively steady release of DA was observed over the next 14 days of incubation, and the cumulative release of DA was near 80%, which showed that the hydrogel coating has a certain ability to control DA release (Fig. 4C). We observed that the solution pH did not change significantly before and after the release of DA (Table

S2). Released DA could continue to affect the bone microenvironment. Therefore, we believe that our method provides an efficient way to control the release of DA from the surfaces of implants.

### 3.5. Identifying the concentration of DA used for drug loading

RAW264.7 cells, a classic model cell line for in vitro studies of osteoclasts, were employed in this study. First, the effect of DA on the differentiation of RAW264.7 cells, osteoclast precursors, was determined to identify the proper concentration of DA for drug loading. We conducted a concentration-response experiment on tissue culture polystyrene (TCPS) by CCK-8 assay to determine a safe concentration of DA for RAW264.7 cells. The results showed that DA at concentrations below 100  $\mu$ M did not affect the proliferation of RAW264.7 cells (Fig. S2). RANKL is a key receptor activator of NF $\kappa$ B ligand and key cytokine required for the survival, proliferation, formation and differentiation of osteoclast precursor cells in vitro. RANKL treatment strongly induces osteoclastogenesis in RAW264.7 cells. Osteoclast differentiation is accompanied by a series of intracellular changes in gene and protein expression [56]. TRAP is a crucial biochemical marker of osteoclasts; its serum concentration acts as a marker of osteoclast function and bone resorption [57]. The TRAP activity assay and TRAP staining results in Fig. S3 show that among safe DA concentrations, DA at a concentration above 100 nM started to inhibit TRAP activity in a concentration-dependent manner ( $p < 0.05$ ). The number of TRAP-positive multinucleated osteoclasts on day 7 was significantly reduced by treatment with 10  $\mu$ M DA but was not substantially reduced with 10 nM DA compared to the corresponding proportion of RANKL-treated RAW264.7 cells. In addition, through qRT-PCR, which is the expression of osteoclast-specific genes, TRAP, MMP-9, Cathepsin K, and NFATc1 were shown to not be significantly affected by 10 nM DA, but their expression levels were downregulated by 10  $\mu$ M DA (Fig. S4A). Cathepsin K is a vital determinant of resorptive activity by osteoclasts and may be partly involved in bone-remodeling diseases [2]. MMP-9 has a direct role in the activation of osteoclastogenic genes by cutting the terminal tail of histone H3N (H3NT) and changing the chromatin structure [58]. NFATc1

mediates osteoclast differentiation and fusion and the degradation of inorganic and organic bone matrices [59]. Thus, western blotting was applied to identify the protein expression level of NFATc1; the results were consistent with those previously reported (Fig. S4B). These findings showed that DA had high biological safety. Based on these results, we applied a concentration of DA of 10  $\mu\text{M}$  for loading in the low-concentration group for follow-up experiments.

### 3.6. Survival and proliferation of RAW264.7 cells on interfaces

Calcein-AM and PI were employed to determine the ratio of live/dead cells and analyze the viability of RAW264.7 cells on the interfaces (Fig. 5A). Live cell membranes bound calcein-AM and appeared green, and dead cell nuclei were stained with PI and appeared red [39]. After 2 days of culture, most of the cells in all groups were stained green, except the group treated with 10 mM DA, indicating that the viability was good. Compared with those in the hydrogel-modified group, the cells on SLA titanium were more likely to aggregate into clusters of osteoclasts. Aggregation is conducive to osteoclast differentiation [60]. We counted the number of live/dead cells to determine cell viability (Fig. 5B). The survival rates of the cells in each group were  $82.56\% \pm 0.91\%$ ,  $81.35\% \pm 0.99\%$ ,  $83.03\% \pm 0.98\%$ ,  $81.92\% \pm 2.01\%$ ,  $81.69\% \pm 0.57\%$ , and  $64.37\% \pm 1.53\%$ . Significant differences in survival rate were observed between the 10 mM DA-treated group and other groups ( $p < 0.01$ ). The CCK-8 assay was utilized to evaluate the proliferative ability of RAW264.7 cells on the interfaces. The results showed that on the 4th and 7th days, the proliferation of RAW264.7 cells on the surfaces of the hydrogel-modified materials was slightly inhibited compared to that of the SLA group. Similar to the previous results of the experiment conducted with TCPS, DA at the appropriate loading concentration (10–1000  $\mu\text{M}$ ) did not affect cell proliferation (Fig. 5C). However, after the loading concentration of DA reached 10 mM, the proliferative ability of the cells was significantly affected, likely because the high drug-loading concentration caused the early release of DA at a high concentration. Therefore, in a follow-up functional experiment, we discarded the group treated with DA at a loading concentration greater than 10 mM. These results showed that the viability of RAW264.7 cells cultured on the surfaces of hydrogen coatings loaded with DA at the proper

concentration (approximately 1000  $\mu\text{M}$ ) was not affected, the cells did not easily aggregate, and the proliferation rate was slightly decreased.

### 3.7. Expression of genes and proteins related to osteoclastogenesis in RAW264.7 cells at the interfaces

TRAP activity assays showed that continuous stimulation of the modified hydrogel group without DA loading with RANKL reduced TRAP activity on the 4th and 7th days and that DA (100  $\mu\text{M}$  and 1000  $\mu\text{M}$  groups) loading further inhibited TRAP activity in a concentration-dependent manner (Fig. 6A–B). The qRT-PCR results on the 7th day demonstrated that DA inhibited the expression of osteoclast-specific genes (Cathepsin K, MMP-9, NFATc1 and TRAP) (Fig. 6C).

The formation of F-actin is considered to be a prerequisite for the resorption of bone tissue by osteoclasts [61]. The phalloidin immunofluorescence staining results revealed that cells on the surface of the SLA showed a clear, large, F-actin ring, indicating the formation of a sealing zone and the strong ability to dissolve the bone matrix, but formation of the F-actin ring was restricted on hydrogel-modified titanium surfaces and further downregulated by DA (Fig. 6D). NFATc1 activation and nuclear translocation have leading roles in the transcriptional regulation of osteoclastogenesis marker genes (TRAP, MMP-9 and cathepsin K) related to osteoclast differentiation. To evaluate the effect of the interfaces on the activation of NFATc1 induced by RANKL, immunofluorescence staining was employed to examine the expression and nuclear translocation of NFATc1. The immunofluorescence staining results shown in Fig. 6E show that the expression and nuclear translocation of NFATc1 were distinctly weakened in the groups administered 100  $\mu\text{M}$  and 1000  $\mu\text{M}$  AlgR@DA. These results indicate that the sodium AlgR-modified hydrogel coating inhibited the maturation and differentiation of osteoclasts and formation of the sealing zone. In addition, DA further inhibited this process and reduced the nuclear translocation of NFATc1. These in vitro results indicated that the modification might have the potential of the hydrogel to inhibit osteoclastogenic activity when it was implanted in vivo.

DA receptors are divided into two subgroups: D1-like receptors (D1 and D5) and D2-like receptors (D2, D3 and D4). Although osteoclasts express all five receptors, Hanami et al. showed that DA inhibits the

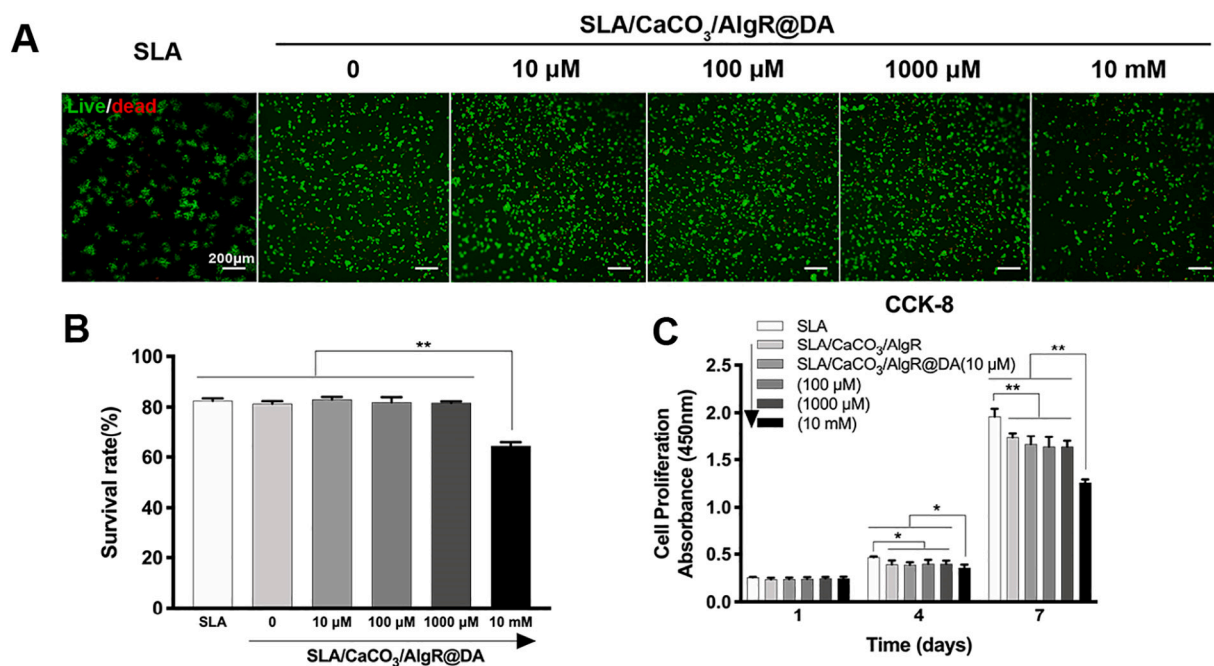
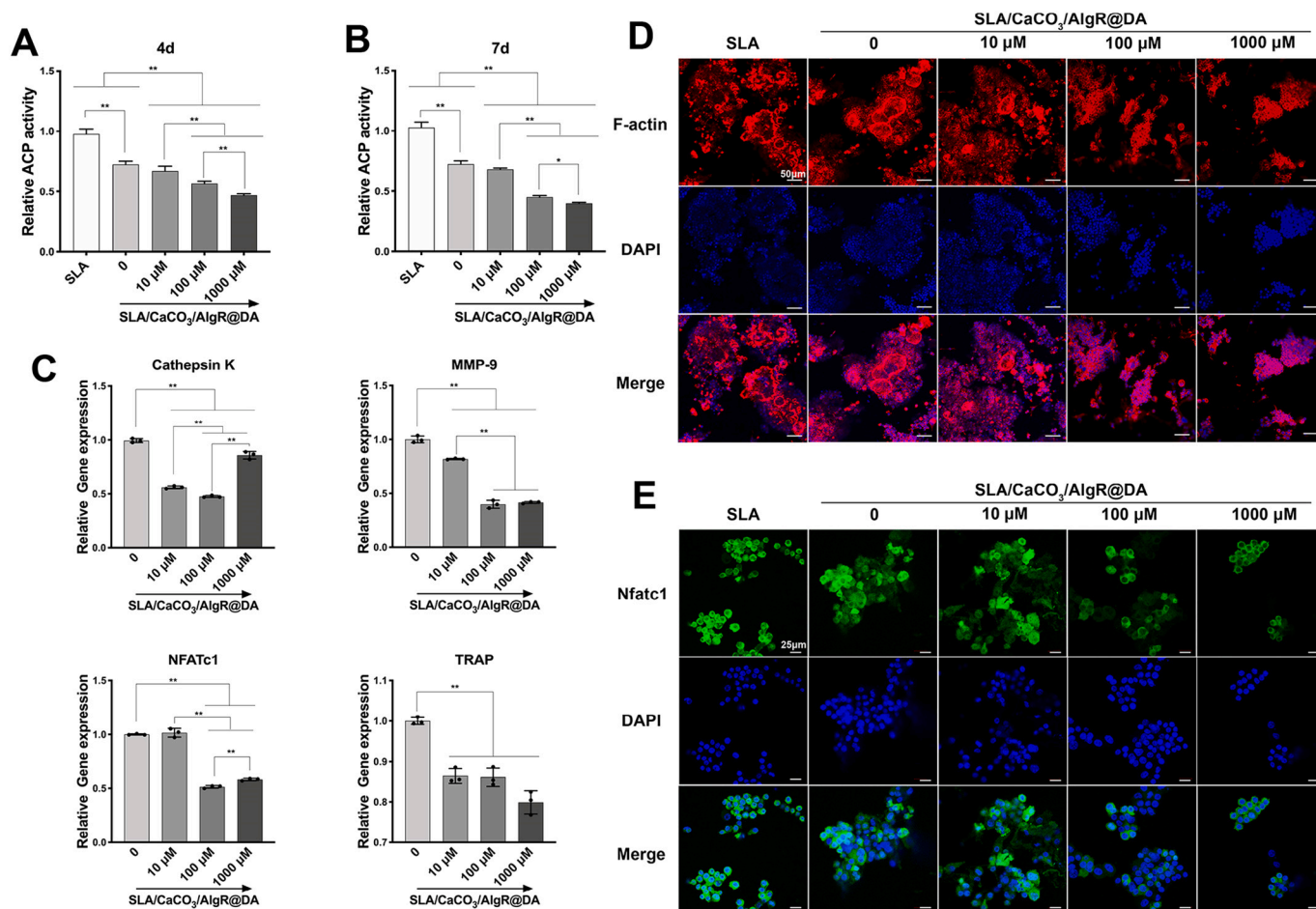


Fig. 5. Survival and proliferation of RAW264.7 cells on different interfaces. Representative live/dead staining images (A) and results of cell viability assays (B) after 48 h of culture (scale bar: 200  $\mu\text{m}$ ,  $**p < 0.01$ ). (C) Proliferation of RAW264.7 cells after 1, 4 and 7 days ( $*p < 0.05$ ,  $**p < 0.01$ ).



**Fig. 6.** Effect of different interfaces on TRAP activity and osteoclast-specific gene expression in RANKL-induced RAW264.7 cells. (A–B) TRAP activity after 4 and 7 days of culture. (C) qRT-PCR analysis of osteoclast-specific genes after 7 days: Cathepsin K, MMP-9, NFATc1, and TRAP. (D) F-actin staining of osteoclasts after 4 days (scale bar: 50 μm). (E) In-situ immunofluorescence staining for NFATc1 on day 7 (scale bar: 25 μm).

formation and function of osteoclasts through only D2-like receptors [15,16]. Thus, we verified the effects of DA in RAW264.7 cells under our culture conditions. The qRT-PCR results showed that from the first to the 7th day, D1R and D2R were expressed in RAW264.7 cells and upregulated during RANKL-induced osteoclastogenesis (Fig. S5). Next, siRNA transfection was applied to knock down D1R and D2R expression in RAW264.7 cells. The qRT-PCR results showed that the inhibitory effect of DA on the differentiation of RAW264.7 cells into osteoclasts was significantly inhibited by D2R knockdown (Fig. S6). We then added 5 μM DA, 1 μM SKF-38393 (a D1R agonist) or 10 μM pramipexole (a D2R agonist) to RAW264.7 osteoclast differentiation media. As shown in Fig. S7A, when pramipexole was added to the media, TRAP activity significantly decreased, and the number of TRAP-positive multinucleated osteoclasts was significantly reduced, which were equivalent to the effects in DA-stimulated cells. In contrast, SKF-38393 seemed to have almost no effect on the osteoclastogenesis of RAW264.7 cells. Consistent with these results, qRT-PCR analysis revealed that the mRNA expression levels of osteoclast-specific genes were downregulated by only DA or pramipexole treatment (Fig. S7B). In summary, these results clarified that DA-induced inhibition of the osteoclast differentiation of RAW264.7 cells was mediated by the activation of D2R.

### 3.8. Different mechanisms of controlled DA release and traditional, free, DA administration

The binding of RANKL and RANK is a key step in the development of

osteoclasts, as it triggers several crucial downstream signaling pathways. Previous research has shown that Akt phosphorylation promotes the activation of NFκB, which can be transferred to the nucleus, where it regulates the expression of different genes and affects the survival of osteoclasts [62,63]. In addition, cAMP response element binding protein (CREB) is a mediator of the cAMP signaling pathway that is activated by PKA [64]. A recent study showed that CREB is essential for inducing the transcription of c-Fos and NFATc1 during osteoclastogenesis [65]. The latest research has revealed that PKA-CREB mediates the inhibitory effects of DA during osteoclastogenesis [66]. DA-mediated D2R activation can cause the phosphorylation of Akt or PKA, depending on whether the G-protein has dissociated from D2R [67]. Additionally, the opposing effects of AKT and PKA after the activation of D2R were shown to regulate GH4T2 cell proliferation [68]. Therefore, we identified the effect of DA released from the AlgR@DA coating and traditional, free administration on these two signaling pathways.

RAW264.7 cells cultured on SLA administered 1 μM DA were utilized as a control. After 7 days of RANKL-induced osteoclastogenesis, cellular proteins were extracted from RAW264.7 cells on SLA and AlgR@DA-modified SLA. SLA and hydrogel-coated interfaces without DA loading were applied as controls. The results of the western blot analysis shown in Fig. 7A–B demonstrate that the AlgR@DA coating downregulated the protein expression of NFATc1 on the 7th day.

The results in Fig. 7C–D show the mechanism of dopamine in the inhibition of osteoclastogenesis. DA administered as a free agent inhibited the phosphorylation of PKA and CREB via the activation of a classic G-protein-dependent D2 receptor signaling pathway, which led

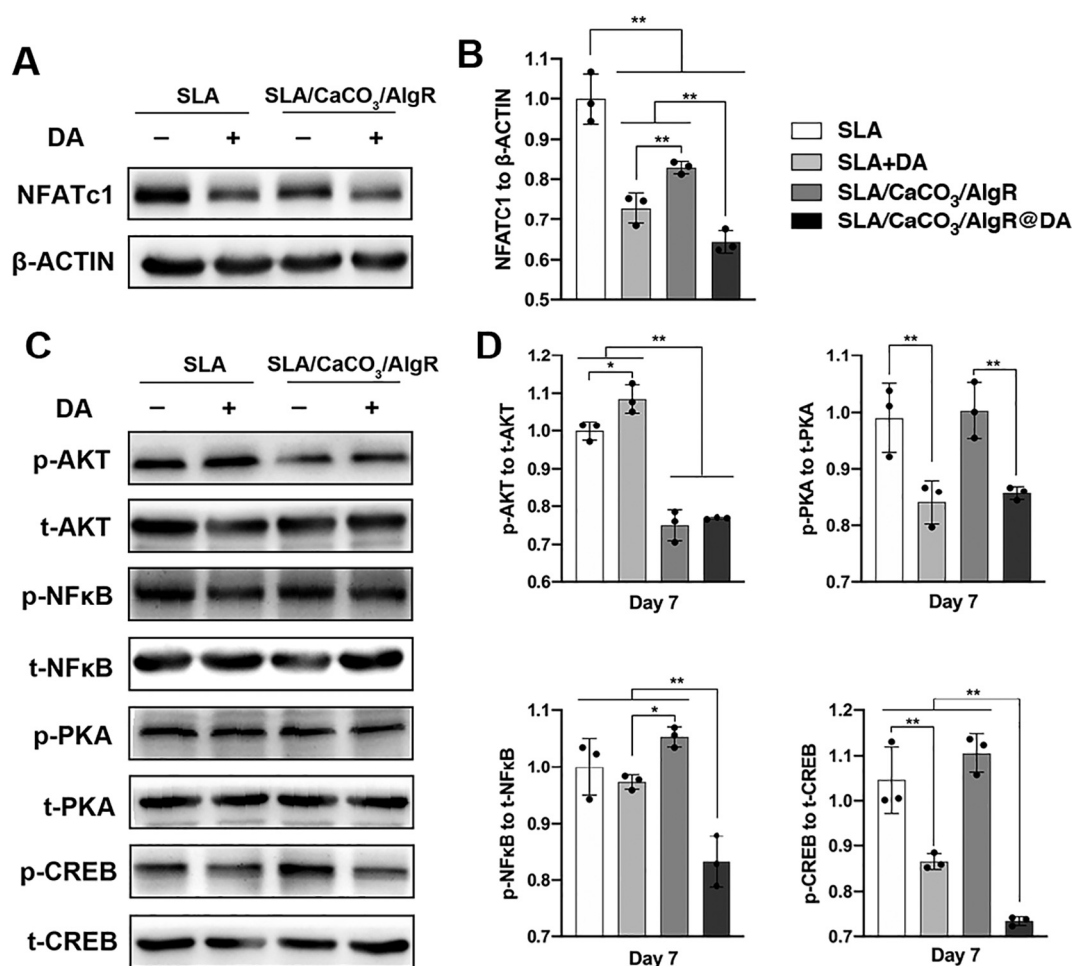


**Fig. 7.** Proteins associated with osteoclastogenesis, including those in the AKT/NFκB pathways and PKA/CREB signaling, in RANKL-induced RAW264.7 DA cells through controlled release or the traditional, free drug administration method. (A–B) Western blot analysis to assess changes in NFATc1 protein expression after 7 days ( $*p < 0.05$ ,  $**p < 0.01$ ). (C–D) Western blot and semiquantitative analyses of p-Akt, p-NFκB, p-PKA, and p-CREB levels after 7 days of induction. t-Akt, t-NFκB, t-PKA, and t-CREB served as internal reference proteins ( $*p < 0.05$  and  $**p < 0.01$ ).

to the decreased expression of NFATc1 and further suppressed the differentiation of osteoclasts. This research is consistent with previous research [66]. In addition, we discovered that the opposite regulation of AKT phosphorylation after DA was given directly in vitro or by AlgR hydrogel coating since the nonloaded AlgR hydrogel coating inhibited AKT phosphorylation. Interestingly, we noticed that DA released from AlgR@DA inhibited not only phosphorylation of PKA and CREB but also phosphorylation of AKT and NF-κB, which caused a decrease in NFATc1. These changes might explain why the DA released from AlgR@DA showed the lowest expression of NFATc1 and the most significant inhibition of osteoclast differentiation (Fig. 7A–B). This result may be attributed to the notion that DA-mediated D2R activation upon traditional, free, DA administration also causes a decrease in voltage-dependent Ca<sup>2+</sup> channel currents, negatively regulating D2R activation [69]. However, when Ca<sup>2+</sup> is displaced from alginate coatings in an ion-rich microenvironment, it can regulate Ca<sup>2+</sup> channels [45]. Therefore, further research is needed to determine how to control D2R activation. To the best of our knowledge, most of the studies on drug delivery systems have explored their effects via drug models. This study used DA for drug delivery via implants to regulate bone homeostasis; the results proved that DA showed ideal biocompatibility and that DA released from materials in a controlled fashion had a better inhibitory effect than DA administered via traditional, free, drug administration. We could also draw the same conclusion from the results of a western blot analysis of the protein expression level of NFATc1 (Fig. 7A–B).

### 3.9. hBMSC responses to DA-loaded hydrogel coatings on titanium

To determine the optimal concentration of DA-loaded materials to regulate the balance between bone resorption and osteogenesis, we conducted assays on hBMSCs. BMSCs are derived from a mesodermal cell line with self-renewal and multidifferentiation potential. They can differentiate into osteoblasts, chondrocytes and other mesenchymal cell types. This process is affected by the characteristics of the interfaces in contact with the cell [70]. We investigated the effects of the coatings on the proliferation, adhesion and osteogenic differentiation of hBMSCs. As shown in the live/dead staining and SEM results in Fig. 8A and C, compared with SLA, more cells with better adhesion and spreading were observed in the hydrogel-coated group on the first day of culture. The DA-loaded group showed more pseudopodia with greater spreading mainly because both the grafted RGD ligands and DA promoted cell adhesion [42,43,55]. The results of the live/dead staining and CCK-8 assays revealed that the hydrogel coating had a minimal effect on the proliferation of hBMSCs, while a high concentration of DA (10 mM) significantly inhibited the proliferation of hBMSCs (Fig. 8A–B). This phenomenon was also observed in RAW264.7 cells (Fig. 5A–C). To study the effect of the DA-loaded coatings on osteogenic differentiation, we tested the ALP activity of hBMSCs after osteogenic induction. Studies have shown that DA can activate receptors on the surfaces of osteogenic precursor cells and promote osteogenic differentiation of cells [13]. ALP has a major role in bone mineralization and is considered to be a

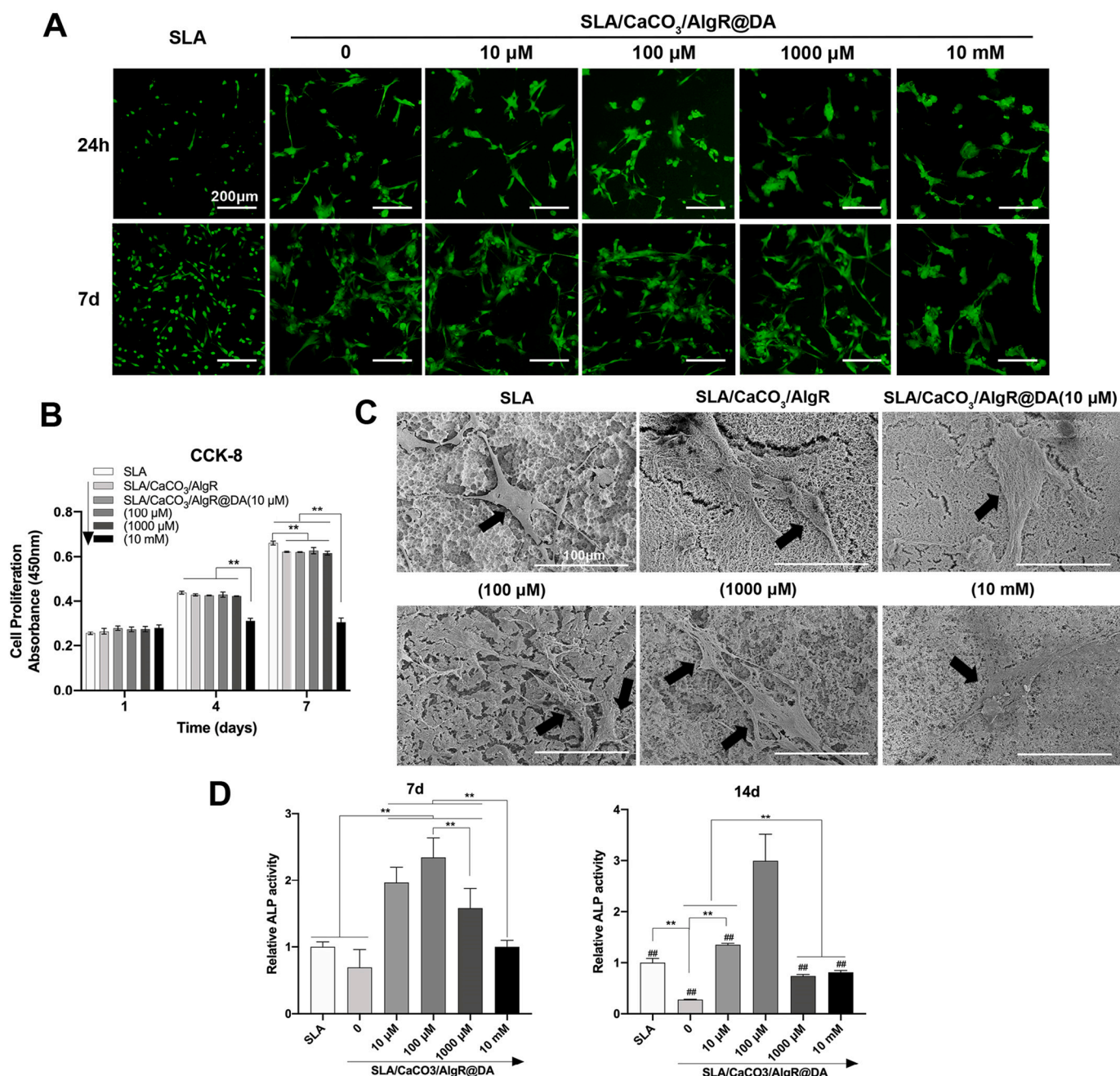


**Fig. 8.** hBMSC responses to DA-loaded hydrogel coatings on titanium. (A) Representative live/dead staining images of hBMSCs on different interfaces for 24 h and 7 days (scale bar: 200  $\mu\text{m}$ ). (B) Proliferation of hBMSCs after 1, 4 and 7 days by CCK-8 (\*\* $p < 0.01$ ). (C) SEM images of hBMSCs grown on different interfaces for 24 h (hBMSCs are indicated by black arrows, scale bar: 100  $\mu\text{m}$ ). (D) ALP activity of hBMSCs (\* $p < 0.05$ , \*\* $p < 0.01$ , ## $p < 0.01$  relative to the 100  $\mu\text{M}$  DA-loaded group).

phenotypic differentiation marker of osteoblasts [19]. As shown in Fig. 8D, on the 7th day of induction, compared with the SLA and DA-unloaded groups, higher ALP activity was observed in the DA-loaded groups. The promotion effect on osteogenic differentiation was the best in the 10  $\mu\text{M}$  and 100  $\mu\text{M}$  DA-loaded groups. On the 14th day, the ALP activity of the 100  $\mu\text{M}$  DA group was the highest. This finding is consistent with our previous results that low concentrations of DA can promote the osteogenic differentiation of BMSCs [18]. These experimental results illustrate that for the osteogenic differentiation of BMSCs, loading a suitable concentration of DA hydrogel coating to continuously deliver DA can promote a osteogenic response and that the promotion effect is best when the loading concentration is 100  $\mu\text{M}$  in this coating.

In this study, in vitro results showed that control-released DA can not only inhibit osteoclastic activity but also promote osteogenesis, thereby

accelerating bone remodeling, as shown in Fig. 9. The optimal DA-loaded concentration of this bidirectional regulation is 100  $\mu\text{M}$ .

As an endogenous small molecule substance, DA has the characteristics of rapid metabolism in the body, and it is difficult to accumulate an effective concentration. The use of a slow-release system can be fully utilized and shows sequential release characteristics. From the perspective of cellular and molecular mechanisms, osteoclast precursor cells colonize the defect surface in the early stage of osteogenesis and then recruit mesenchymal stem cells to differentiate into osteoblasts. DA initially has the physiological characteristics of osteoclasts and then exhibits the physiological characteristics of bone formation. The early release of DA in this gel coating can not only increase the concentration of local DA and affect the differentiation of osteoclasts but also promote the adhesion of stem cells. A small amount of DA is released slowly, and

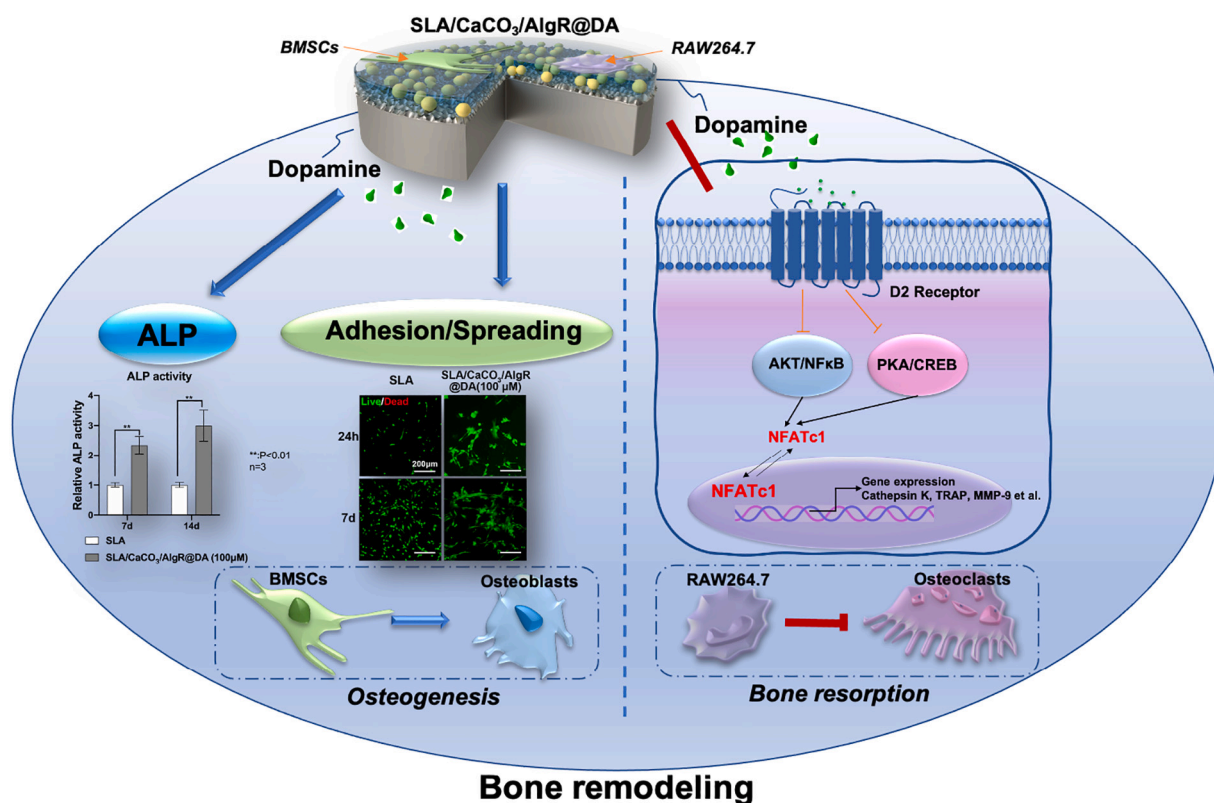


Fig. 9. Schematic of the regulation of DA-loaded hydrogel coating materials on bone remodeling by enhancing osteogenesis and attenuating bone resorption.

the local low concentration of DA effectively promotes the differentiation of mesenchymal stem cells. Compared with common bone repair materials (such as bone growth factors, bisphosphonate drugs and apatite), DA acts as a natural small compound in the bone marrow and is milder. Previous studies have proven the safety of alginate hydrogels and DA [15,23,71]. These findings provide a new perspective for the preparation of bone implanting materials. However, this study had several limitations. First, it was not clear whether the release behavior of DA in vivo was similar to that in vitro. Second, this study did not verify the osseointegration effect of the materials in vivo. The in vivo environment is more complicated, and further optimization of synthesis parameters may be needed. Therefore, the in vivo effectiveness of DA sustained-release coatings needs to be further explored.

#### 4. Conclusion

In this study, we successfully fabricated a bioactive hydrogel layer on a rough titanium surface that continuously and steadily released DA, which is an active small-molecule drug. The experimental results show that the RGD-coupled, alginate hydrogel coating inhibits TRAP activity and that DA released into the microenvironment further impairs the formation and differentiation of osteoclasts while promoting the adhesion and osteogenic differentiation of BMSCs. Based on the results of functional experiments, the optimal DA loading concentration to regulate the balance between bone resorption and osteogenesis is 100  $\mu\text{M}$ . This method has great potential in solving the problems around the implant in patients with metabolic bone-related diseases.

#### CRedit authorship contribution statement

**Mingyue Wang:** Conceptualization, Methodology, Formal analysis, Investigation, Writing – original draft. **Chenxi Wang:** Conceptualization, Methodology, Writing – review & editing. **Yu Zhang:** Conceptualization, Supervision, Funding acquisition. **Ye Lin:** Conceptualization,

Supervision, Funding acquisition.

#### Declaration of competing interest

The authors declare no competing financial interest.

#### Acknowledgments

This paper was financially supported by the National Key R&D Program of China (2018YFC1105302, 2018YFC1105304) and Science Foundation of Peking University School and Hospital of Stomatology (PKUSS) (grant number 20150106). The authors thank Yixiang Wang for his writing assistance.

#### Appendix A. Supplementary data

qRT-PCR primer sequences of genes in RAW264.7 cells (Table S1); The solution pH after DA release (Table S2); EDX spectroscopy results (Fig. S1); CCK-8 of different concentration of DA on RAW264.7 cells (Fig. S2); TRAP activity and staining assay of DA on RANKL-induced RAW264.7 cells (Fig. S3); qRT-PCR analysis and western blot of DA on RANKL-induced RAW264.7 cells (Fig. S4); D1R and D2R expression (Fig. S5); transfection with D1 or D2 receptor-specific siRNAs (Fig. S6); and D1 and D2 receptor agonists on RAW264.7 cells osteoclastogenesis (Fig. S7). Supplementary data to this article can be found online at <https://doi.org/10.1016/j.msec.2021.112376>.

#### References

- [1] B. Langdahl, S. Ferrari, D.W. Dempster, Bone modeling and remodeling: potential as therapeutic targets for the treatment of osteoporosis, *Ther. Adv. Musculoskelet. Dis.* 8 (6) (2016) 225–235.
- [2] T.D. Rachner, S. Khosla, L.C. Hofbauer, Osteoporosis: now and the future, *Lancet* 377 (9773) (2011) 1276–1287.
- [3] X. Feng, J.M. McDonald, Disorders of bone remodeling, *Annu. Rev. Pathol.* 6 (2011) 121–145.

- [4] T. Ono, T. Nakashima, Recent advances in osteoclast biology, *Histochem. Cell Biol.* 149 (4) (2018) 325–341.
- [5] A. Barik, N. Chakravorty, Targeted drug delivery from titanium implants: a review of challenges and approaches, *Adv. Exp. Med. Biol.* 1251 (2020) 1–17.
- [6] A.C. Anselmo, S. Mitragotri, An overview of clinical and commercial impact of drug delivery systems, *J. Control. Release* 190 (2014) 15–28.
- [7] S. Khosla, L.C. Hofbauer, Osteoporosis treatment: recent developments and ongoing challenges, *Lancet Diab. Endocrinol.* 5 (11) (2017) 898–907.
- [8] Y. Zeng, M. Zhou, L. Chen, H. Fang, S. Liu, C. Zhou, J. Sun, Z. Wang, Alendronate loaded graphene oxide functionalized collagen sponge for the dual effects of osteogenesis and anti-osteoclastogenesis in osteoporotic rats, *Bioact. Mater.* 5 (4) (2020) 859–870.
- [9] X. Shen, P. Ma, Y. Hu, G. Xu, K. Xu, W. Chen, Q. Ran, L. Dai, Y. Yu, C. Mu, K. Cai, Alendronate-loaded hydroxyapatite-TiO<sub>2</sub> nanotubes for improved bone formation in osteoporotic rabbits, *J. Mater. Chem. B* 4 (8) (2016) 1423–1436.
- [10] C. Dharmayanti, T.A. Gillam, D.B. Williams, A. Blencowe, Drug-eluting biodegradable implants for the sustained release of bisphosphonates, *Polymers (Basel)* 12 (12) (2020).
- [11] S.B. Woo, J.W. Hellstein, J.R. Kalmar, Systematic review: bisphosphonates and osteonecrosis of the jaws, *Ann. Intern. Med.* 144 (10) (2006) 753–761.
- [12] C. Missale, S.R. Nash, S.W. Robinson, M. Jaber, M.G. Caron, Dopamine receptors: from structure to function, *Physiol. Rev.* 78 (1) (1998) 189–225.
- [13] D.J. Lee, H.C. Tseng, S.W. Wong, Z. Wang, M. Deng, C.C. Ko, Dopaminergic effects on in vitro osteogenesis, *Bone Res* 3 (2015) 15020.
- [14] K.J. Motyl, M. Beauchemin, D. Barlow, P.T. Le, K. Nagano, A. Treyball, A. Contractor, R. Baron, C.J. Rosen, K.L. Houseknecht, A novel role for dopamine signaling in the pathogenesis of bone loss from the atypical antipsychotic drug risperidone in female mice, *Bone* 103 (2017) 168–176.
- [15] H. Yang, Y. Xu, M. Zhu, Y. Gu, W. Zhang, H. Shao, Y. Wang, Z. Ping, X. Hu, L. Wang, D. Geng, Inhibition of titanium-particle-induced inflammatory osteolysis after local administration of dopamine and suppression of osteoclastogenesis via D2-like receptor signaling pathway, *Biomaterials* 80 (2016) 1–10.
- [16] K. Hanami, K. Nakano, K. Saito, Y. Okada, K. Yamaoka, S. Kubo, M. Kondo, Y. Tanaka, Dopamine D2-like receptor signaling suppresses human osteoclastogenesis, *Bone* 56 (1) (2013) 1–8.
- [17] S. Liu, Y. Fan, A. Chen, A. Jalali, K. Minami, K. Ogawa, H. Nakshatri, B.Y. Li, H. Yokota, Osteocyte-driven downregulation of snail restrains effects of Drd2 inhibitors on mammary tumor cells, *Cancer Res.* 78 (14) (2018) 3865–3876.
- [18] C.X. Wang, X.Y. Ge, M.Y. Wang, T. Ma, Y. Zhang, Y. Lin, Dopamine D1 receptor-mediated activation of the ERK signaling pathway is involved in the osteogenic differentiation of bone mesenchymal stem cells, *Stem Cell Res Ther* 11 (1) (2020) 12.
- [19] M. Wang, X. Ge, Y. Zheng, C. Wang, Y. Zhang, Y. Lin, Microarray analysis reveals that lncRNA PWRN1-209 promotes human bone marrow mesenchymal stem cell osteogenic differentiation on microtopography titanium surface in vitro, *J. Biomed. Mater. Res. B Appl. Biomater.* 108 (7) (2020) 2889–2902.
- [20] L.-C. Zhang, L.-Y. Chen, L. Wang, Surface modification of titanium and titanium alloys: technologies, developments, and future interests, *Adv. Eng. Mater.* 22 (5) (2020).
- [21] T.N. Gevrek, A. Degirmenci, R. Sanyal, A. Sanyal, Multifunctional and transformable ‘clickable’ hydrogel coatings on titanium surfaces: from protein immobilization to cellular attachment, *Polymers (Basel)* 12 (6) (2020).
- [22] X. Yin, L. Yan, D. Jun Hao, S. Liu, M. Yang, B. He, Z. Liu, Calcium alginate template-mineral substituted hydroxyapatite hydrogel coated titanium implant for tibia bone regeneration, *Int. J. Pharm.* 582 (2020) 119303.
- [23] Z. Luo, S. Zhang, J. Pan, R. Shi, H. Liu, Y. Lyu, X. Han, Y. Li, Y. Yang, Z. Xu, Y. Sui, E. Luo, Y. Zhang, S. Wei, Time-responsive osteogenic niche of stem cells: a sequentially triggered, dual-peptide loaded, alginate hybrid system for promoting cell activity and osteo-differentiation, *Biomaterials* 163 (2018) 25–42.
- [24] K. Huang, J. Wu, Z. Gu, Black phosphorus hydrogel scaffolds enhance bone regeneration via a sustained supply of calcium-free phosphorus, *ACS Appl. Mater. Interfaces* 11 (3) (2019) 2908–2916.
- [25] J. Gacanian, A. Kovtun, S. Fischer, V. Schwager, J. Quambusch, S.L. Kuan, W. Liu, F. Boldt, C. Li, Z. Yang, D. Liu, Y. Wu, T. Weil, H. Barth, A. Ignatius, Spatiotemporally controlled release of rho-inhibiting C3 toxin from a protein-DNA hybrid hydrogel for targeted inhibition of osteoclast formation and activity, *Adv. Healthc. Mater.* 6 (21) (2017).
- [26] A. Concheiro, C. Alvarez-Lorenzo, Chemically cross-linked and grafted cyclodextrin hydrogels: from nanostructures to drug-eluting medical devices, *Adv. Drug Deliv. Rev.* 65 (9) (2013) 1188–1203.
- [27] D.W. Grainger, C.H. Greff, P. Gong, M.J. Lochhead, Current microarray surface chemistries, *Methods Mol. Biol.* 381 (2007) 37–57.
- [28] J.A. Rowley, G. Madlambayan, D.J. Mooney, Alginate hydrogels as synthetic extracellular matrix materials, *Biomaterials* 20 (1) (1999) 45–53.
- [29] M.S. Savel'yeva, A.A. Abalymov, G.P. Lyubun, I.V. Vidyasheva, A.M. Yashchenok, T.E. Douglas, D.A. Gorin, B.V. Parakhonskiy, Vaterite coatings on electrospun polymeric fibers for biomedical applications, *J. Biomed. Mater. Res. A* 105 (1) (2017) 94–103.
- [30] Y. Xin, Y. Liu, D. Liu, J. Li, C. Zhang, Y. Wang, S. Zheng, New function of RUNX2 in regulating osteoclast differentiation via the AKT/NFATc1/CTSK axis, *Calcif. Tissue Int.* 106 (5) (2020) 553–566.
- [31] D.L. Cochran, D. Buser, C.M. ten Bruggenkate, D. Weingart, T.M. Taylor, J. P. Bernard, F. Peters, J.P. Simpson, The use of reduced healing times on ITI implants with a sandblasted and acid-etched (SLA) surface: early results from clinical trials on ITI SLA implants, *Clin. Oral Implants Res.* 13 (2) (2002) 144–153.
- [32] B.V. Muir, D. Myung, W. Knoll, C.W. Frank, Grafting of cross-linked hydrogel networks to titanium surfaces, *ACS Appl. Mater. Interfaces* 6 (2) (2014) 958–966.
- [33] H. Yuk, T. Zhang, S. Lin, G.A. Parada, X. Zhao, Tough bonding of hydrogels to diverse non-porous surfaces, *Nat. Mater.* 15 (2) (2016) 190–196.
- [34] R. Major, K. Trembecka-Wojciga, M. Kot, J.M. Lackner, P. Wilczek, B. Major, In vitro hemocompatibility on thin ceramic and hydrogel films deposited on polymer substrate performed in arterial flow conditions, *Mater. Sci. Eng. C Mater. Biol. Appl.* 61 (2016) 15–22.
- [35] V.A. Koshuro, G.G. Nechaev, A.V. Lyasnikova, Composition and structure of coatings formed on a VT16 titanium alloy by electro-plasma spraying combined with microarc oxidation, *Tech. Phys.* 59 (10) (2014) 1570–1572.
- [36] J. Yang, R. Bai, B. Chen, Z. Suo, Hydrogel adhesion: a supramolecular synergy of chemistry, topology, and mechanics, *Adv. Funct. Mater.* 30 (2) (2019).
- [37] C. Muderrisoglu, M. Saveleva, A. Abalymov, L. Van der Meeren, A. Ivanova, V. Atkin, B. Parakhonskiy, A.G. Skirtach, Nanostructured biointerfaces based on bio ceramic calcium carbonate/hydrogel coatings on titanium with an active enzyme for stimulating osteoblasts growth, *Adv. Mater. Interfaces* 5 (19) (2018).
- [38] Z. Zhao, W. Gao, H. Bai, A mineral layer as an effective binder to achieve strong bonding between a hydrogel and a solid titanium substrate, *J. Mater. Chem. B* 6 (23) (2018) 3859–3864.
- [39] Z. Wu, Q. Li, S. Xie, X. Shan, Z. Cai, In vitro and in vivo biocompatibility evaluation of a 3D bioprinted gelatin-sodium alginate/rat Schwann-cell scaffold, *Mater. Sci. Eng. C Mater. Biol. Appl.* 109 (2020) 110530.
- [40] K.Y. Lee, S.H. Yuk, Polymeric protein delivery systems, *Prog. Polym. Sci.* 32 (7) (2007) 669–697.
- [41] R. Detsch, B. Sarker, T. Zehnder, A.R. Boccaccini, T.E.L. Douglas, Additive manufacturing of cell-loaded alginate enriched with alkaline phosphatase for bone tissue engineering application, *BioNanoMaterials* 15 (2014) 3–4.
- [42] M. Barczyk, S. Carracedo, D. Gullberg, Integrins, *Cell Tissue Res.* 339 (1) (2010) 269–280.
- [43] F. Martino, A.R. Perestrelo, V. Vinarsky, S. Pagliari, G. Forte, Cellular mechanotransduction: from tension to function, *Front. Physiol.* 9 (2018) 824.
- [44] Hyväri L, Ojansivu M, Juntunen M, Kartasalo K, Miettinen S, Vanhatupa S. Focal adhesion kinase and ROCK signaling are switch-like regulators of human adipose stem cell differentiation towards osteogenic and adipogenic lineages. *Stem Cells Int.* 2018;2018:1–13.
- [45] Alginate hydrogel and aerogel, *Alginates* (2019) 59–77.
- [46] Z. Schwartz, K. Kieswetter, D.D. Dean, B.D. Boyan, Underlying mechanisms at the bone-surface interface during regeneration, *J. Periodontol. Res.* 32 (1 Pt 2) (1997) 166–171.
- [47] A. Kozbial, Z. Li, C. Conaway, R. McGinley, S. Dhingra, V. Vahdat, F. Zhou, B. D'Urso, H. Liu, L. Li, Study on the surface energy of graphene by contact angle measurements, *Langmuir* 30 (28) (2014) 8598–8606.
- [48] T. Albrektsson, A. Wennerberg, The impact of oral implants — past and future, 1966–2042, *J. Can. Dent. Assoc.* 71 (5) (2005) 327.
- [49] L. Nouri, S. Hemidouche, A. Boudjema, F. Kaouah, Z. Sadaoui, K. Bachari, Elaboration and characterization of photobiocomposite beads, based on titanium (IV) oxide and sodium alginate biopolymer, for basic blue 41 adsorption/ photocatalytic degradation, *Int. J. Biol. Macromol.* 151 (2020) 66–84.
- [50] C. Qu, Z. Bao, X. Zhang, Z. Wang, J. Ren, Z. Zhou, M. Tian, X. Cheng, X. Chen, C. Feng, A thermosensitive RGD-modified hydroxybutyl chitosan hydrogel as a 3D scaffold for BMSCs culture on keloid treatment, *Int. J. Biol. Macromol.* 125 (2019) 78–86.
- [51] A. Thakur, S. Ranote, D. Kumar, K.K. Bhardwaj, R. Gupta, G.S. Chauhan, Synthesis of a PEGylated dopamine ester with enhanced antibacterial and antifungal activity, *ACS Omega* 3 (7) (2018) 7925–7933.
- [52] M. Panouillé, V. Larreta-Garde, Gelation behaviour of gelatin and alginate mixtures, *Food Hydrocoll.* 23 (4) (2009) 1074–1080.
- [53] J.D. Kaunitz, Yamaguchi DT, TNAP, TRAP, ecto-purinergic signaling, and bone remodeling, *J. Cell. Biochem.* 105 (3) (2008) 655–662.
- [54] R. Durán, M. Alfonso, B. Arias, Determination of biogenic amines in rat brain dialysates by high performance liquid chromatography, *J. Liq. Chromatogr. Relat. Technol.* 21 (18) (2006) 2799–2811.
- [55] S. Chen, B. Bai, D.J. Lee, S. Diachina, Y. Li, S.W. Wong, Z. Wang, H.C. Tseng, C. K. Ko, Dopaminergic enhancement of cellular adhesion in bone marrow derived mesenchymal stem cells (MSCs), *J. Stem Cell Res. Ther.* 7 (8) (2017).
- [56] D.L. Lacey, E. Timms, H.L. Tan, M.J. Kelley, C.R. Dunstan, T. Burgess, R. Elliott, A. Colombero, G. Elliott, S. Scully, H. Hsu, J. Sullivan, N. Hawkins, E. Davy, C. Capparelli, A. Eli, Y.X. Qian, S. Kaufman, I. Sarosi, V. Shalhoub, G. Senaldi, J. Guo, J. Delaney, W.J. Boyle, Osteoprotegerin ligand is a cytokine that regulates osteoclast differentiation and activation, *Cell* 93 (2) (1998) 165–176.
- [57] M. Li, X. Chen, J. Yan, L. Zhou, Y. Wang, F. He, J. Lin, C. Zhu, G. Pan, J. Yu, M. Pei, H. Yang, T. Liu, Inhibition of osteoclastogenesis by stem cell-derived extracellular matrix through modulation of intracellular reactive oxygen species, *Acta Biomater.* 71 (2018) 118–131.
- [58] K. Kim, Y. Shin, J. Kim, T.S. Ulmer, W. An, H3K27me1 is essential for MMP-9-dependent H3N-terminal tail proteolysis during osteoclastogenesis, *Epigenetics Chromatin* 11 (1) (2018) 23.
- [59] H. Takayanagi, S. Kim, T. Koga, H. Nishina, M. Isshiki, H. Yoshida, A. Saiura, M. Isobe, T. Yokochi, J. Inoue, E.F. Wagner, T.W. Mak, T. Kodama, T. Taniguchi, Induction and activation of the transcription factor NFATc1 (NFAT2) integrate RANKL signaling in terminal differentiation of osteoclasts, *Dev. Cell* 3 (6) (2002) 889–901.
- [60] X. Feng, S.L. Teitelbaum, Osteoclasts: new insights, *Bone Res.* 1 (1) (2013) 11–26.
- [61] D. Georgess, I. Machuca-Gayet, A. Blangy, P. Jurdic, Podosome organization drives osteoclast-mediated bone resorption, *Cell Adhes. Migr.* 8 (3) (2014) 191–204.

- [62] A. Gingery, E. Bradley, A. Shaw, M.J. Oursler, Phosphatidylinositol 3-kinase coordinately activates the MEK/ERK and AKT/NFkappaB pathways to maintain osteoclast survival, *J. Cell. Biochem.* 89 (1) (2003) 165–179.
- [63] R. Inoue, N.A. Matsuki, G. Jing, T. Kanematsu, K. Abe, M. Hirata, The inhibitory effect of alendronate, a nitrogen-containing bisphosphonate on the PI3K-Akt-NFkappaB pathway in osteosarcoma cells, *Br. J. Pharmacol.* 146 (5) (2005) 633–641.
- [64] Y. Koga, H. Tsurumaki, H. Aoki-Saito, M. Sato, M. Yatomi, K. Takehara, T. Hisada, Roles of cyclic AMP response element binding activation in the ERK1/2 and p38 MAPK signalling pathway in central nervous system, cardiovascular system, osteoclast differentiation and mucin and cytokine production, *Int. J. Mol. Sci.* 20 (6) (2019).
- [65] D.Z. Lu, W. Dong, X.J. Feng, H. Chen, J.J. Liu, H. Wang, L.Y. Zang, M.C. Qi, CaMKII ( $\delta$ ) regulates osteoclastogenesis through ERK, JNK, and p38 MAPKs and CREB signalling pathway, *Mol. Cell. Endocrinol.* 508 (2020) 110791.
- [66] L. Wang, L. Han, P. Xue, X. Hu, S.W. Wong, M. Deng, H.C. Tseng, B.W. Huang, C. C. Ko, Dopamine suppresses osteoclast differentiation via cAMP/PKA/CREB pathway, *Cell. Signal.* 78 (2021) 109847.
- [67] J.M. Beaulieu, S. Espinoza, R.R. Gainetdinov, Dopamine receptors — IUPHAR review 13, *Br. J. Pharmacol.* 172 (1) (2015) 1–23.
- [68] A.K. Roof, S. Jirawatnotai, T. Trudeau, C. Kuzyk, M.E. Wierman, H. Kiyokawa, A. Gutierrez-Hartmann, The balance of PI3K and ERK signaling is dysregulated in prolactinoma and modulated by dopamine, *Endocrinology* 159 (6) (2018) 2421–2434.
- [69] M. Liu, L. Ren, X. Zhong, Y. Ding, T. Liu, Z. Liu, X. Yang, L. Cui, L. Yang, Y. Fan, Y. Liu, Y. Zhang, D2-like receptors mediate dopamine-inhibited insulin secretion via ion channels in rat pancreatic  $\beta$ -cells, *Front. Endocrinol. (Lausanne)* 11 (2020) 152.
- [70] F. Rastegar, D. Shenaq, J. Huang, W. Zhang, B.Q. Zhang, B.C. He, L. Chen, G. W. Zuo, Q. Luo, Q. Shi, E.R. Wagner, E. Huang, Y. Gao, J.L. Gao, S.H. Kim, J. Z. Zhou, Y. Bi, Y. Su, G. Zhu, J. Luo, X. Luo, J. Qin, R.R. Reid, H.H. Luu, R. C. Haydon, Z.L. Deng, T.C. He, Mesenchymal stem cells: molecular characteristics and clinical applications, *World J. Stem Cells* 2 (4) (2010) 67–80.
- [71] H. Wang, C. Lin, X. Zhang, K. Lin, X. Wang, S.G. Shen, Mussel-inspired polydopamine coating: a general strategy to enhance osteogenic differentiation and osseointegration for diverse implants, *ACS Appl. Mater. Interfaces* 11 (7) (2019) 7615–7625.